J|A|C|S ARTICLES

Published on Web 05/19/2010

Membrane-Mediated Effect on Ion Channels Induced by the Anesthetic Drug Ketamine

Hansjörg Jerabek,[†] Georg Pabst,*[,‡] Michael Rappolt,[‡] and Thomas Stockner*[,†,§]

Department of Heath & Environment, Austrian Institute of Technology, A-2444 Seibersdorf, Austria, Institute of Biophysics and Nanosystems Research, Austrian Academy of Sciences, A-8042 Graz, Austria, and Center for Pathobiochemistry and Genetics, Department of Medical Chemistry, Medical University of Vienna, A-1090 Vienna, Austria

Received December 23, 2009; E-mail: thomas.stockner@meduniwien.ac.at; georg.pabst@oeaw.ac.at

Abstract: Anesthetic drugs have been in use for over 160 years in surgery, but their mode of action remains largely unresolved. We have studied the effect of (*R*)-(−)-ketamine on the biophysical properties of lipid model membranes composed of palmitoyloleoylphosphatidylcholine by a combination of X-ray diffraction and all-atom molecular dynamics simulations. In agreement with several previous studies, we do not find significant changes to the membrane thickness and lateral area per lipid up to 8 mol % ketamine content. However, we observed that the insertion of ketamine within the lipid/water interface caused significant changes of lateral pressure and a pressure shift toward the center of the bilayer. The changes are predicted to be large enough to affect the opening probability of ion channels as derived for two protein models. Depending on the protein model, we found inhibition values of $IC_{50} = 2$ mol % and 18 mol % ketamine, corresponding to approximately 0.08 and 0.9 μM concentrations in the blood circulation, respectively. This compares remarkably well with clinical applied concentrations. We thus provide evidence for a lateral pressure mediated mode of anesthesia, first proposed more than 10 years ago.

Introduction

General anesthetic drugs were introduced more than 160 years ago[1] and are indispensable in daily surgery at hospitals. In view of this remarkable track record, it comes as a surprise that our knowledge on the mode of action of these important drug molecules remains limited. Thus far, consensus has been reached only in two aspects: (i) general anesthetics act on the central nervous system (brain and spinal cord) and (ii) modulate activity of a large number of ion channels of the neurotransmission system (see, e.g., reviews[2−6]). Investigation into the molecular site(s) of interaction of anesthetics has led to one of the most controversial debates of scientific history. At present, there are two schools, one favoring specific (direct) interactions of the drugs with the target proteins[4] and a second adhering to nonspecific mechanisms through a modulation of biophysical membrane properties.[7−10] However, the protein and lipid hypotheses are not necessarily mutually exclusive in view of the well-known interdependencies of proteins and lipids in cellular function.[11−13]

In the present work, we studied a bilayer-mediated mechanism that was proposed by Cantor[10] more than 10 years ago, but which has never been tested rigorously against experimental and simulation data. The central element of this hypothesis is the lateral pressure profile of lipid membranes, which results from a minimization of the membrane free energy with respect to the lateral area per lipid molecule.[14] The lateral pressure profile $p_{LAT}(z)$ describes the balance of attractive and repulsive pressures (interactions) at a given depth z across the lipid bilayer.

Anesthetics are well-known for their partitioning into lipid bilayers[15,16] and hence may shift the lateral pressure within the lipid bilayer, in particular if they locate close to the lipid−water interface, where $p_{LAT}(z)$ changes from positive to negative values. Based on thermodynamic arguments, Cantor showed theoretically how this may affect the activity of membrane proteins if their conformational change involves a nonuniform

[†] Austrian Institute of Technology.
[‡] Austrian Academy of Sciences.
[§] Medical University of Vienna.

(1) Eckenhoff, R. G. *Mol. Interv.* **2001**, *1*, 258–268.
(2) Urban, B. W. *Br. J. Anaesth.* **2002**, *89*, 167–183.
(3) Mashour, G. A.; Forman, S. A.; Campagna, J. A. *Best Pract. Res. Clin. Anaesthesiol.* **2005**, *19*, 349–364.
(4) Franks, N. P. *Br. J. Pharmacol.* **2006**, *147* (Suppl. 1), S72–S81.
(5) Hendrickx, J. F.; Eger, E. I.; Sonner, J. M.; Shafer, S. L. *Anesth. Analg.* **2008**, *107*, 494–506.
(6) Eger, E. I.; Raines, D. E.; Shafer, S. L.; Hemmings, H. C. J.; Sonner, J. M. *Anesth. Analg.* **2008**, *107*, 832–848.
(7) Ueda, I. *Keio J. Med.* **2001**, *50*, 20–25.
(8) Heimburg, T.; Jackson, A. D. *Biophys. J.* **2007**, *92*, 3159–3165.
(9) Wodzinska, K.; Blicher, A.; Heimburg, T. *Soft Matter* **2009**, *5*, 3319–3330.
(10) Cantor, S. R. *Biochemistry* **1997**, *36*, 2339–2344.
(11) Simons, K.; Ikonen, E. *Nature* **1997**, *387*, 569–572.
(12) van Meer, G.; Voelker, D. R.; Feigenson, G. W. *Nat. Rev. Mol. Cell Biol.* **2008**, *9*, 112–124.
(13) Escriba, P. V.; Gonzalez-Ros, J. M.; Goni, F. M.; Kinnunen, P. K.; Vigh, L.; Sanchez-Magraner, L.; Fernandez, A. M.; Busquets, X.; Horvath, I.; Barcelo-Coblijn, G. *J. Cell. Mol. Med.* **2008**, *12*, 829–875.
(14) Ben Shaul, A. Molecular theory of chain packing, elasticity and lipid-protein interaction in lipid bilayers. In *Handbook of Biological Physics*; Lipowsky, R., Sackmann, E., Eds.; Elsevier: Amsterdam., 1995; Vol. 1, pp 359−401.
(15) Overton, C. E. *Studien über die Narkose. Zugleich ein Beitrag zur allgemeinen Pharmakologie*; G. Fischer Verlag: Jena, 1901.
(16) Meyer, H. H. *Arch. Exp. Pathol. Pharmakol.* **1899**, *42*, 109–118.

 10.1021/ja910843d

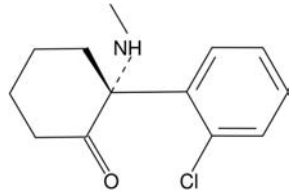

Figure 1. Chemical structure of (*R*)-(−)-ketamine.

lateral change of their cross-sectional area throughout the lipid membrane.[17]

Verifying the proposed mechanism has proved challenging because lateral pressure profiles were so far experimentally not accessible on an absolute scale.[18] Nevertheless, recent all-atom molecular dynamics (MD) simulations of lipid bilayers demonstrated their capability to derive $p_{LAT}(z)$,[19−21] showing the effects of cholesterol, alcohols, and lipid composition.[22−27] For validation, however, simulations need to be compared to experimental observables on membrane properties.[28−31]

In this work, we combined MD simulations with small-angle X-ray diffraction (SAXD) to show for the first time that the intravenously administered anesthetic drug ketamine (Figure 1) has a strong influence on the lateral pressure in phospholipid membranes at clinically relevant concentrations. In particular, we focused on the (*R*)-(−) enantiomer of ketamine which was shown to be about four times less effective than its clinically used (*S*)-(+) form,[32] adding a further challenge to the sensitivity of the applied techniques.

Materials and Methods

Model Membranes. 1-Palmitoyl-2-oleoylphosphatidylcholine (POPC) was purchased from Avanti Polar Lipids (Alabaster, AL) and (±)-2-(2-chlorophenyl)-2-(methylamino)cyclohexanone hydrochloride (ketamine) from Sigma-Aldrich (St. Louis, MO) and used without further purification. (*R*)-(−)-ketamine is not commercially available. The ketamine used throughout the experiments is therefore a racemic mixture. However, the derived changes in membrane structure upon the addition of ketamine are so small (see below) that we can exclude significant different results for (*R*)-(−)-ketamine.

Lipid membranes were prepared by first mixing appropriate amounts of lipid and drug stock solutions (solvent: methanol/chloroform (2/1 v/v)). The organic solvent was removed by using first a gentle stream of N_2 and subsequently a vacuum chamber (∼8 h), which yielded dry lipid films containing (0, 2, 4, and 8 mol %) ketamine. Fully hydrated multilamellar vesicles (MLVs) were obtained by dispersing the dry lipid films in 18 MΩ/cm water at a concentration of 50 mg/mL using vigorous intermittent vortex mixing.

Experimental Techniques and Analysis. SAXD experiments were performed at the Austrian SAXS beamline at the synchrotron source Elettra (Trieste, Italy) using 8 keV photons. X-ray patterns were recorded with a mar345 (Marresearch, Norderstedt, Germany) image plate detector, and scattering angles were calibrated using silver behenate. MLVs were contained in thin-walled quartz-glass capillaries (diameter: 1 mm) and equilibrated at 310 K using a circulating water bath (Unistat CC, Huber, Offenburg, Germany) for 10 min prior to each measurement. The sample-to-detector distance was 1.39 m, and the X-ray exposure time for each samples was 300 s.

The program Fit2D (http://www.esrf.eu/computing/scientific/FIT2D/) was used for primary data reduction. The background corrected SAXD patterns were further analyzed in the full q-range (scattering vector $q = 4\pi \sin(\theta)/\lambda$, 2θ is the scattering angle, λ represents the wavelength) using a previously described global model.[33−35] The most relevant parameters for the comparison with MD simulations obtained from this analysis are the form factor $F(q)$, membrane thickness d_B, and lateral area per lipid A.

$F(q)$ is given by the Fourier transform using a simple model for the electron density profile of the lipid bilayer, as[33]

$$F_{exp}(q) = \sqrt{2\pi}[2\sigma_H \exp(-\sigma_H^2 q^2/2) \cos(qz_H) - \sigma_C \rho_C \exp(-\sigma_C^2 q^2/2)] \quad (1)$$

where z_H is the position of the headgroup Gaussian of width σ_H, σ_C the width of the Gaussian modeling of the electron-sparse methyl terminus of the hydrocarbon chains, and ρ_C is its amplitude relative to the amplitude of the headgroup Gaussian. The scattered intensity of the MLVs also contains the structure factor $S(q)$ to account for the positional correlations of the bilayers and reads as

$$I(q) = \frac{S(q)|F_{exp}(q)|^2}{q^2} \quad (2)$$

We used a structure factor according to the modified Caillé theory, as described previously.[33,34] Our approach of combining MD simulations with SAXS data differs from procedures applied by other groups, which derive the experimental form factor directly, i.e., model-free, from unilamellar vesicles.[28−31] Instead, we used MLVs and applied eq 1 using a simple Gaussian model to represent the electron density profile. The advantage of using MLVs is that the lamellar repeat distance d, which is directly reported, is very sensitive to membrane structure and bilayer interactions, thus providing an additional parameter for drug/lipid interactions. It has been demonstrated previously that different electron density models for lipid bilayers give an equally good description of the form factor;[35] i.e., they fit the experimental data equally well. Hence, we expect that our form factors differ only marginally from model-free experimental form factors as determined from unilamellar vesicles.[28−31]

The lateral area per lipid is calculated from $A = (V_L - V_H)/d_C$,[35] where $V_L = 1.26$ nm^3 is the molecular volume of POPC at

(17) Cantor, R. S. *Chem. Phys. Lipids* **1999**, *101*, 45–56.
(18) Templer, R. H.; Castle, S. J.; Curran, A. R.; Rumbles, G.; Klug, D. R. *Faraday Discuss.* **1998**, *111*, 41–53.
(19) Lindahl, E.; Edholm, O. *J. Chem. Phys.* **2000**, *113*, 3882–3893.
(20) Sonne, J.; Hansen, F. Y.; Peters, G. H. *J. Chem. Phys.* **2005**, *122*, 124903.
(21) Gullingsrud, J.; Schulten, K. *Biophys. J.* **2004**, *86*, 3496–3509.
(22) Edholm, O.; Nyberg, A. M. *Biophys. J.* **1992**, *63*, 1081–1089.
(23) Terama, E.; Ollila, O. H. S.; Salonen, E.; Rowat, A. C.; Trandum, C.; Westh, P.; Patra, M.; Karttunen, M.; Vattulainen, I. *J. Phys. Chem. B* **2008**, *112*, 4131–4139.
(24) Ollila, O. H. S.; Róg, T.; Karttunen, M.; Vattulainen, I. *J. Struct. Biol.* **2007**, *159*, 311–323.
(25) Ollila, O. H. S.; Hyvönen, M. T.; Vattulainen, I. *J. Phys. Chem. B* **2007**, *111*, 3139–3150.
(26) Griepernau, B.; Böckmann, R. A. *Biophys. J.* **2008**, *95*, 5766–5778.
(27) Hofsäss, C.; Lindahl, E.; Edholm, O. *Biophys. J.* **2003**, *84*, 2192–2206.
(28) Sachs, J. N.; Petrache, H. I.; Woolf, T. B. *Chem. Phys. Lipids* **2003**, *126*, 211–223.
(29) Klauda, J. B.; Kucerka, N.; Brooks, B. R.; Pastor, R. W.; Nagle, J. F. *Biophys. J.* **2006**, *90*, 2796–2807.
(30) Pandit, S. A.; Chiu, S.; Jakobsson, E.; Grama, A.; Scott, H. L. *Biophys. J.* **2007**, *92*, 920–927.
(31) Kucerka, N.; Nagle, J. F.; Sachs, J. N.; Feller, S. E.; Pencer, J.; Jackson, A.; Katsaras, J. *Biophys. J.* **2008**, *95*, 2356–2367.
(32) White, P. F.; Schüttler, J.; Shafer, A.; Stanski, D. R.; Horai, Y.; Trevor, A. J. *Br. J. Anaesth.* **1985**, *57*, 197–203.
(33) Pabst, G.; Rappolt, M.; Amenitsch, H.; Laggner, P. *Phys. Rev. E* **2000**, *62*, 4000–4009.
(34) Pabst, G.; Koschuch, R.; Pozo-Navas, B.; Rappolt, M.; Lohner, K.; Laggner, P. *J. Appl. Crystallogr.* **2003**, *63*, 1378–1388.
(35) Pabst, G. *Biophys. Rev. Lett.* **2006**, *1*, 57–84.

310 K,[36] $V_H = 0.319$ nm^3 the headgroup volume of phosphatidylcholine,[37] and $d_C = z_H - 0.4$ nm[37] is the hydrocarbon chain length.

Simulations. The systems simulated in this work consisted of 200 POPC molecules, 35 water molecules per lipid, and 0−16 (*R*)-(−)-ketamine molecules (Figure 1), inserted into the membrane, corresponding to drug concentrations of 0−8 mol %. The simulation system was constructed from a POPC bilayer downloaded from the Tieleman group (http://moose.bio.ucalgary.ca), enlarged to contain 10 × 10 lipids per leaflet and pre-equilibrated for 5 ns. The ketamines were rotated randomly and placed inside the hydrophobic slab of the membrane bilayer. Atom overlaps were resolved by first expanding the bilayer in the membrane plane, followed by a size reduction in small steps to the typical area per lipid of POPC, involving energy minimization and geometry optimization for each deflation step.[38] This initial system was hydrated with 35 water molecules per lipid and equilibrated by a 50 ns simulation. Subsequently, a 50 ns production run was carried out.

Berger lipids,[39] converted into the format of the OPLS all-atom force field,[40] following the procedure proposed by Neale (Gromacs mailing list; www.pomeslab.com/files/lipidCombinationRules.pdf), were used to describe the POPC molecules. The OPLS all-atom force field was applied for ketamine, and water was represented by the SPC[41] water model. All simulations were performed using the Gromacs 4.0.4 MD package.[42,43] The integration time step was set to 2 fs. Periodic boundary conditions were applied in all dimensions. The neighbor search list was updated every 10 steps. A constant temperature of 310 K was maintained using the velocity rescale (v-rescale) algorithm[44] with a coupling time of 0.1 ps, coupling independently the water and the lipids plus anesthetics to an external bath. A pressure of 1 bar was maintained both in the membrane plane and the membrane normal, using a semi-isotropic Berendsen pressure coupling scheme[45] with a time constant of 4 ps. Bond lengths were constrained using the LINCS method.[46] A cutoff of 1.0 nm was applied for VdW interactions. Long-range electrostatic interactions were calculated according to particle mesh Ewald (PME) method[47] with a cutoff of 1 nm. The reciprocal space interactions were evaluated on a 0.12 nm grid using B-splines of fourth order.

We calculated the form factor from the simulations from[30]

$$F_{MD}(q) = \int_{-h}^{h} (\rho_e(z) - \rho_{e,bulk}) \cos(qz) dz \quad (3)$$

where ρ_e denotes the symmetric electron density of the system, $\rho_{e,bulk}$ is the electron density of water, and the integration limit h corresponds to half of the simulation box in the z-direction.

The membrane thickness used for comparison with SAXD data was defined as the head to headgroup peak distance (d_{HH}), extracted directly from the time-averaged electron density. The area per lipid of POPC molecules was estimated from simulation trajectories after removing the contribution of the ketamine molecules to the area per lipid A by subtracting the volume of the ketamine molecules (0.53 nm^3) from the total membrane volume.

The deuterium order parameter S_{CD} is a measure for the alignment of the carbon deuterium bond vector relative to the bilayer normal z. The order parameter tensor

$$S_{ij} = \frac{1}{2}\langle 3 \cos\theta_i \cos\theta_j - \delta_{ij} \rangle \quad (4)$$

is used to obtain the order parameter. Here, δ_{ij} is the Kronecker delta and θ_i is the angle between the ith molecular axis and the bilayer normal,[48] the average runs over all lipids and time frames. The deuterium-order parameter for a saturated acyl chain carbon is given by

$$S_{CD}^{SAT} = \frac{2S_{xx}}{3} + \frac{S_{yy}}{3} \quad (5)$$

and for an unsaturated carbon by

$$S_{CD}^{UNSAT} = \frac{S_{zz}}{4} + \frac{3S_{yy}}{4} \mp \frac{\sqrt{3}S_{yz}}{2} \quad (6)$$

Lateral Pressure Profiles. Lipid membranes are self-assembled, highly dynamic systems in which the lateral pressure varies considerably along the bilayer normal.[14] Three main interaction regimes can be distinguished: in the headgroup region a positive pressure can be found due to repulsion. In contrast, the cost of free energy associated with the exposure of the apolar hydrocarbon regime leads to a significant lateral attraction close to the headgroup−hydrocarbon interface. In the hydrophobic layer the mutual repulsion of the hydrocarbon chains is dominant and leads to a positive pressure.

Lateral pressure profiles were derived from MD simulations by re-evaluating the raw trajectories with a modified version of Gromacs 4.0.2[49] and by applying the Irving−Kirkwood contour,[50] using the rerun option and the SHAKE method[51] for bond length constraints. Electrostatic interactions were treated using a cutoff of 1.8 nm. For the calculation, the bilayer was subdivided into 0.1 nm thick lateral slices for which the local pressure tensor is given by

$$p_{slice}(z) = p(z) = \frac{1}{\Delta V}\left[\sum_{i \in slice} m_i v_i v_i - \sum_{i<j} F_{ij} r_{ij} f(z, z_i, z_j)\right] \quad (7)$$

where z_i, m_i, v_i, F_{ij}, and r_{ij} are the z-coordinate, mass, velocity, force, and distance, respectively of each slab. ΔV is the volume of the slice. The first sum in eq 7 is taken over all particles in a slice and is proportional to their total kinetic energy. The second term describes the contribution of the particle pair interactions to the pressure (virial term). The function $f(z,z_i,z_j)$ assigns a weight to the virial depending on the position of the two particles i and j relative to the considered slice. Using the components of the local pressure tensor, the lateral pressure is given by

$$p_{LAT} = \frac{p_{xx}(z) + p_{yy}(z)}{2} \quad (8)$$

(36) Hianik, T.; Haburcak, M.; Lohner, K.; Prenner, E.; Paltauf, F.; Hermetter, A. *Colloid Surf. A* **1998**, *139*, 189–197.
(37) Pabst, G.; Katsaras, J.; Raghunathan, V. A.; Rappolt, M. *Langmuir* **2003**, *19*, 1716–1722.
(38) Kandt, C.; Ash, W. L.; Tieleman, D. P. *Methods* **2007**, *41*, 475–488.
(39) Berger, O.; Edholm, O.; Jähnig, F. *Biophys. J.* **1997**, *72*, 2002–2013.
(40) Jorgensen, W.; Maxwell, D.; Tirado-Rives, J. *J. Am. Chem. Soc.* **1996**, *118*, 11225–11236.
(41) Berendsen, H. J. C.; Postma, J. P. M.; van Gunsteren, W. F.; Hermans, J. *Intermolecular Forces* **1981**, 331–342.
(42) Hess, B.; Kutzner, C.; van der Spoel, D.; Lindahl, E. *J. Chem. Theory. Comput.* **2008**, *4*, 435–447.
(43) Van der Spoel, D.; Lindahl, E.; Hess, B.; Groenhof, G.; Mark, A. E.; Berendsen, H. J. C. *J. Comput. Chem.* **2005**, *26*, 1701–1718.
(44) Bussi, G.; Donadio, D.; Parrinello, M. *J. Chem. Phys.* **2007**, *126*, 014101.
(45) Berendsen, H. J. C.; Postma, J. P. M.; van Gunsteren, W. F.; DiNola, A.; Haak, J. R. *J. Chem. Phys.* **1984**, *81*, 3684–3690.
(46) Hess, B.; Bekker, H.; Berendsen, H. J. C.; Fraaije, J. G. E. M. *J. Comput. Chem.* **1997**, *18*, 1463–1472.
(47) Darden, T.; York, D.; Pedersen, L. *J. Chem. Phys.* **1993**, *98*, 10089–10092.
(48) Douliez, J. P.; Ferrarini, A.; Dufourc, E. J. *J. Chem. Phys.* **1998**, *109*, 2513–2518.
(49) Lindahl, E.; Edholm, O. *J. Chem. Phys.* **2000**, *113*, 3882–3893.
(50) Irving, J. H.; Kirkwood, J. G. *J. Chem. Phys.* **1950**, *18*, 817.
(51) Ryckaert, J. P.; Ciccotti, G.; Berendsen, H. J. C. *J. Comput. Phys.* **1977**, *23*, 327–341.

The lateral pressure profiles were smoothed by a spline function and symmetrized with respect to the bilayer center.

Effects on Simple Geometric Protein Models. The change in the lateral pressure profile can be related to the equilibrium distribution of a protein by the volume work that accompany the conformational transition between resting and active state (r → t). Cantor[10] has shown that the fraction of protein in the active state in a membrane with modified lateral pressures $p_{LAT}(z)$ relative to the fraction in a reference membrane environment with $p_{0,LAT}(z)$ is given by

$$f = \frac{1 + K_0}{1 + K} \tag{9}$$

$K_0 = [r]_0/[t]_0$ is the reference conformational equilibrium at $p_{0,LAT}(z)$ and $K = [r]/[t] = K_0 e^{\alpha}$ the conformational equilibrium upon a depth-dependent change in $p_{LAT}(z)$, with

$$\alpha = \frac{1}{k_B T} \int_{-d_B/2}^{d_B/2} \Delta p_{LAT}(z) \Delta A_P(z) dz \tag{10}$$

The integration limit d_B is the steric membrane thickness, which was defined as the headgroup electron density peak plus the corresponding half-width at half-maximum values. This definition allows for properly including the complete membrane slab to correctly estimate the first and second moment of the lateral pressure profile that act on membrane inserted proteins. $\Delta A_P(z)$ denotes the change in the cross-sectional area of the protein that is associated with the conformational transition r → t. Thus, the population between the two states can only be affected by $\Delta p_{LAT}(z)$ if the protein's conformational change involves a nonuniform shift in its cross sectional area. Further, the conformational equilibrium shifts toward inhibition for $\alpha > 0$ ($K > K_0$) and toward activation for $\alpha < 0$ ($K < K_0$).

In the absence of a precise knowledge about the cross-sectional changes of membrane-inserted proteins, one can assume that A_P varies smoothly across the lipid bilayer. In this case, $\Delta A_P(z)$ can be expanded in the power series and eq 10 simplifies to[17]

$$\alpha = \frac{1}{k_B T} \sum_j \Delta P_j \Delta a_j \tag{11}$$

where Δa_j are the coefficients of the power expansion and ΔP_j is the change of the jth integral moment

$$P_j = \int_0^{d_B/2} z^j p_{LAT}(z) dz \tag{12}$$

Ketamine is known to be a potent inhibitor of several ligand gated ion channels such as the *N*-methyl-D-asparate (NMDA) receptors, nicotinic acetylcholine receptors (nAChR), or muscarinic acetylcholine receptors to name but a few.[52] High-resolution structures of bacterial homologues of the pentameric nAChR receptor[53,54] are available, as well as the cryoelectron microscopy structure of the nAChR in the closed state.[55] These data show the nAChR structure and conformational changes, but uncertainties remain, as in the putatively open structure the channel remains blocked by side chain residues. In the absence of a precise knowledge of the involved conformational changes we have therefore applied two simple geometric models for ion channels.[17] Both protein models are assumed to consist of an *n*-mer association of α-helices, with a radially symmetric pore-opening.

The conformational change r → t of the first model involves a cooperative tilt of the helices by the angle $\Delta\phi_a = \phi_a^t - \phi_a^r$ with the axis of rotation located at the center of the bilayer (Figure 2A). This rotation opens a pore located at the cytosolic side of the membrane. For this scenario, Cantor[17] has shown that

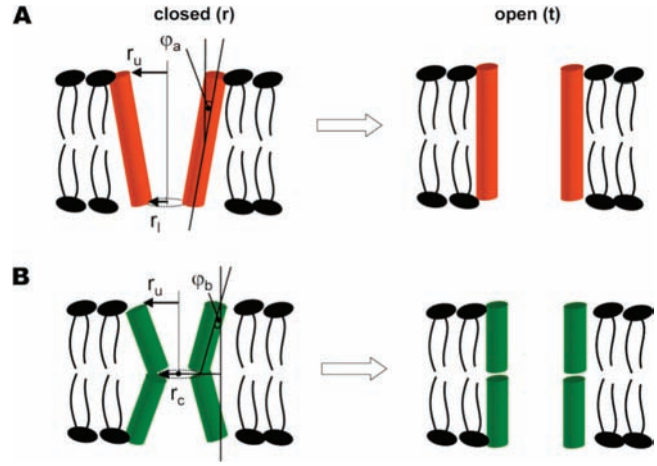

Figure 2. Schematic illustration of the conformational transition of an ion channel from the closed to the open state using the geometric model of tilted (A) and of bent (B) helices.

$$\alpha = \frac{2\pi}{k_B T} (\sin^2(\varphi_a^t) - \sin^2(\varphi_a^r)) \Delta P_2 \tag{13}$$

which means that the change of conformational equilibrium depends only on $\Delta\phi_a$ and on the difference of the second integral moments ΔP_2 of $p_{LAT}(z)$. Given the structural differences reported for the pentameric ion-channel,[53,54] the tilted-helix model can be taken as a first approximation of such a protein.

The r → t mechanism of the second protein model involves an unbending of the helices of an hourglass-shaped form by an angle $\Delta\phi_b$ or a change in relative helical orientation, opening a pore at the center of the bilayer (Figure 2B). Further, this conformational change is assumed to proceed symmetric with respect to $z = 0$. Note that the initial model for bent helix proteins used by Cantor[17] had a fixed central pore with a variable width of outer pore radius r_u. For the present model, Pabst et al.[56] have recently shown that

$$\alpha = \frac{2\pi}{k_B T} \{[2r_u(\tan\varphi_b^t - \tan\varphi_b^r) - d_B(\tan^2\varphi_b^t - \tan^2\varphi_b^r)]\Delta P_1 + (\tan^2\varphi_b^t - \tan^2\varphi_b^r)\Delta P_2\} \tag{14}$$

Here, α depends on ΔP_1 and ΔP_2, on the channel radius, on the extra-cellular side r_u, and on the membrane thickness.

Results

Comparison between Simulation and Experiments. We combined SAXD and MD simulation studies on the present systems in order to validate the simulation results. All experiments and simulations were performed at physiological temperature (310 K) and within the same concentration range of ketamine. Figure 3 shows a snapshot from our simulation trajectory at a concentration of 4 mol % (*R*)-(−)-ketamine. The orientation of the ketamine molecules in the membrane is typical for all simulations. We observed that the carbonyl and the amine functional groups are oriented preferentially toward the hydrophilic−hydrophobic interface with on average 0.7 ± 0.2 hydrogen bonds per (*R*)-(−)-ketamine molecule. The plane of

(52) Sinner, B.; Graf, B. M. Ketamine. In *Modern Anesthetics*; Schüttler, J., Schwilden, H., Eds.; Springer: New York, 2008; pp 313−333.
(53) Hilf, R. J. C.; Dutzler, R. *Nature* **2009**, *457*, 115–118.
(54) Hilf, R. J. C.; Dutzler, R. *Nature* **2008**, *452*, 375–379.
(55) Unwin, N. *J. Mol. Biol.* **2005**, *346*, 967–989.
(56) Pabst, G.; Boulgaropoulos, B.; Gander, E.; Sarangi, B. R.; Amenitsch, H.; Raghunathan, V. A.; Laggner, P. *J. Membr. Biol.* **2009**, *231*, 125–132.

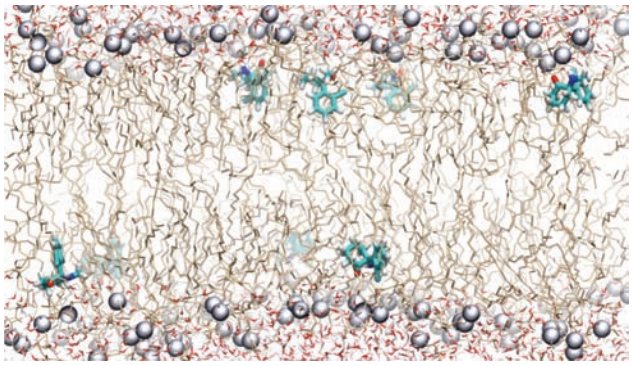

Figure 3. Representative snapshot of the simulation with 4 mol % of ketamine.

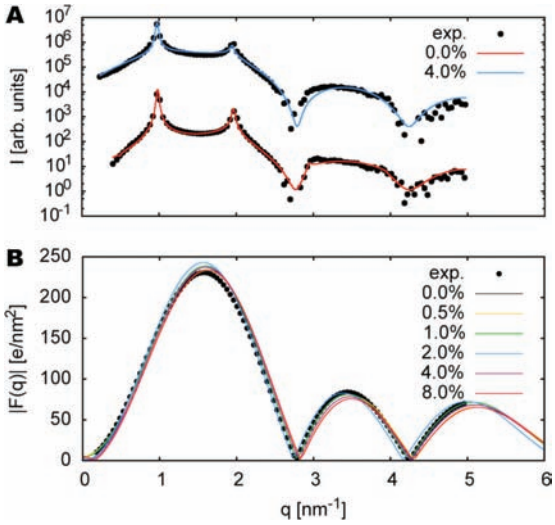

Figure 4. (A) SAXS diffraction patterns of POPC in the absence and presence of ketamine. The solid lines show global fits to the diffraction data. (B) Comparison between the experimentally derived form factor of the unanesthetized membrane and the form factors calculated from the simulation data for various ketamine concentrations. For clarity, a fit to the experimental data is shown only at zero ketamine concentration.

the aromatic ring is typically oriented perpendicular to the plane of the membrane with an average angle between the normals to both planes of 80 ± 35°. The aromatic ring of ketamine inserts deeper into the membrane than the aliphatic ring with the average angle between the membrane normal and the bond joining the two rings of 145 ± 30°.

Figure 4A shows selected SAXD patterns of POPC in the absence and presence of ketamine. Despite some small increase of diffuse intensity (broadening of the Bragg peaks), little influence upon the insertion of ketamine was observed. Additionally, the lamellar repeat distance of the MLVs increased only from 6.39 nm to ~6.45 nm for all tested ketamine concentrations. Figure 4B presents the comparison between the form factor derived from SAXD measurements and the form factors calculated from MD trajectories. The form factors extracted from experiments were put on the same scale as the theoretical $F(q)$ by a multiplication factor. We observe good agreement with respect to the form factor zeros, form factor shape, as well as the location and amplitude of the form factor maxima, respectively.

For further validation of the simulations, we compared the areas per lipid A and the head to headgroup (d_{HH}) thicknesses. In the absence of ketamine, both parameters were found to agree

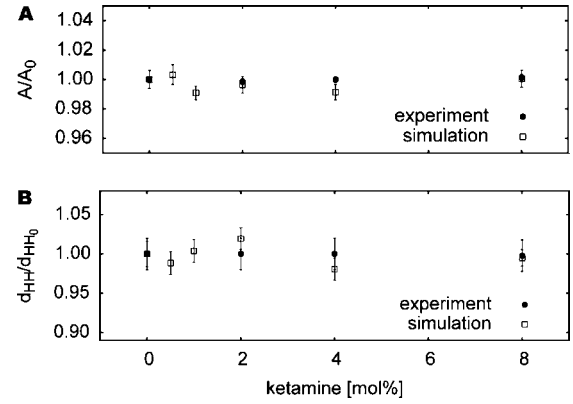

Figure 5. (A) Concentration dependence of the POPC area per lipid relative to the ketamine free membrane A_0 obtained from experiments and simulations. (B) Membrane thickness obtained from experiments and simulations with increasing ketamine concentrations relative to the bilayer free of ketamine d_{HH0}.

well with previous reports.[57−59] However, their absolute values differ slightly, e.g., at 0 mol % ketamine we find $d_{HH}^{exp} = 3.66 \pm 0.02$ nm/$d_{HH}^{sim} = 3.61 \pm 0.06$ nm and $A^{exp} = 0.668 \pm 0.005$ nm^2/$A^{sim} = 0.657 \pm 0.006$ nm^2. This is mainly related to uncertainties in defining the hydrocarbon chain length.[35] Additionally, parametrization of the applied MD force field may also contribute to the differences on absolute scales.[60] It is therefore better to compare changes of d_{HH} and A induced by the presence of the anesthetic drug ketamine on a reduced scale (Figure 5). We found good agreement between simulation and experiment of drug-induced effect. While serving as a confirmation of the MD simulations, our results even more importantly show that the addition of up to 8 mol % drug molecules does not induce measurable changes in area per lipid and membrane thickness.

Ketamine Location, Order Parameter Profiles, And Lateral Pressure Profiles. Electron density distributions, derived from MD simulations (Figure 6), showed that the drug partitions into a narrow region within the membrane, which is close to the headgroup−hydrocarbon interface. Ketamine is mainly hydrophobic, but its polar carbonyl and amine function keeps the drug adjacent to the hydrophilic region. In particular, the peaks of the ketamine distributions were located close to the fifth carbon of the oleoyl chain of POPC (Figure 6B), and their positions were found to be concentration independent.

The calculated deuterium order parameters of the palmitoyl and the oleoyl chain (Figure 7) of pure POPC bilayers are in good agreement with experimental reports.[61,62] Order parameters of both acyl chains increased upon the addition of ketamine, peaking at the position of the fifth carbon atom, in agreement with the location of the drug within the membrane. These results indicate that it might be possible to detect changes in order parameters.

(57) Böckmann, R.; Hac, A.; Heimburg, T.; Grubmüller, H. *Biophys. J.* **2003**, *85*, 1647–1655.
(58) Pabst, G.; Hodzic, A.; Strancar, J.; Danner, S.; Rappolt, M.; Laggner, P. *Biophys. J.* **2007**, *93*, 2688–2696.
(59) Kucerka, N.; Gallova, J.; Uhrikova, D.; Balgavy, P.; Bulacu, M.; Marrink, S. J.; Katsaras, J. *Biophys. J.* **2009**, *97*, 1926–1932.
(60) Chiu, S.-E.; Pandit, S. A.; Scott, H. L.; Jakobsson, E. *J. Phys. Chem. B* **2009**, *119*, 2748–63.
(61) Seelig, J.; Waespe-Sarcevic, N. *Biochemistry* **1978**, *17*, 3310–3315.
(62) Huber, T.; Rajamoorthi, K.; Kurze, V. F.; Beyer, K.; Brown, M. F. *J. Am. Chem. Soc.* **2002**, *124*, 298–309.
(63) Franks, N. P.; Lieb, W. R. *Nature* **1994**, *367*, 607–614.

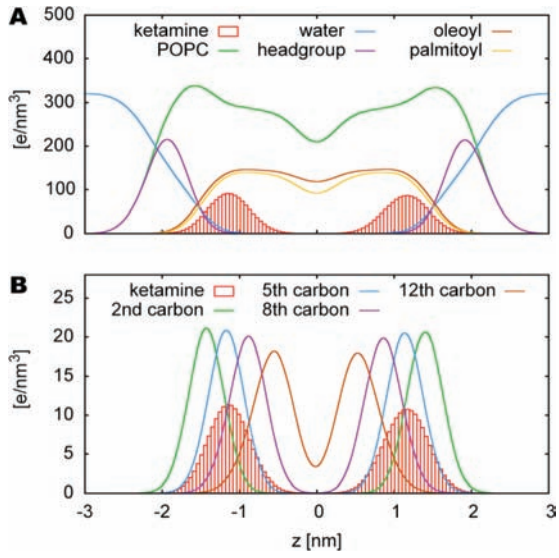

Figure 6. (A) Depth-dependent electron density profile of the simulated membrane at a ketamine concentration of 4 mol %; the ketamine density (red) has been scaled to highlight its position. (B) Comparison between the electron densities of several selected oleoyl chain carbon atoms and the electron density of ketamine.

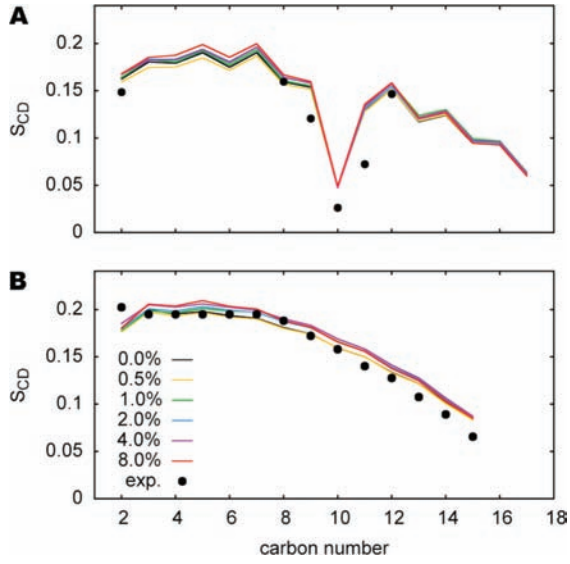

Figure 7. Comparison of the lipid order parameter between experiment and simulations of the (A) oleoyl chain and (B) the palmitoyl chain. Experimental-order parameter of the oleoyl chain have been determined at 40 °C by Seelig et al.;[61] data for the palmitoyl chain are taken from Huber et al.[62] at 37 °C.

The effect of (*R*)-(−)-ketamine on the lateral pressure profiles of POPC bilayers is shown in Figure 8. Despite the insignificant effects of the drug on membrane structural parameters (see above), mirrored also in the almost unchanged position of the positive $p_{LAT}(z)$ peak at $|z| = 2$ nm, ketamine led to strong changes of lateral pressures around $|z| \sim 1.2$ nm, i.e., at the peak position of the ketamine distribution within the bilayer. At this location, $p_{LAT}(z)$ is reduced by ∼100 bar at 4 mol % and ∼200 bar at 8 mol % ketamine. Overall, ketamine caused a net shift of lateral pressures from the polar/apolar interface toward the center of the lipid bilayer.

First (P_1) and second moments (P_2) derived from the lateral pressure profiles depend on the applied integration limit (see eq 12) as displayed in Figure 8B for pure POPC bilayers. The

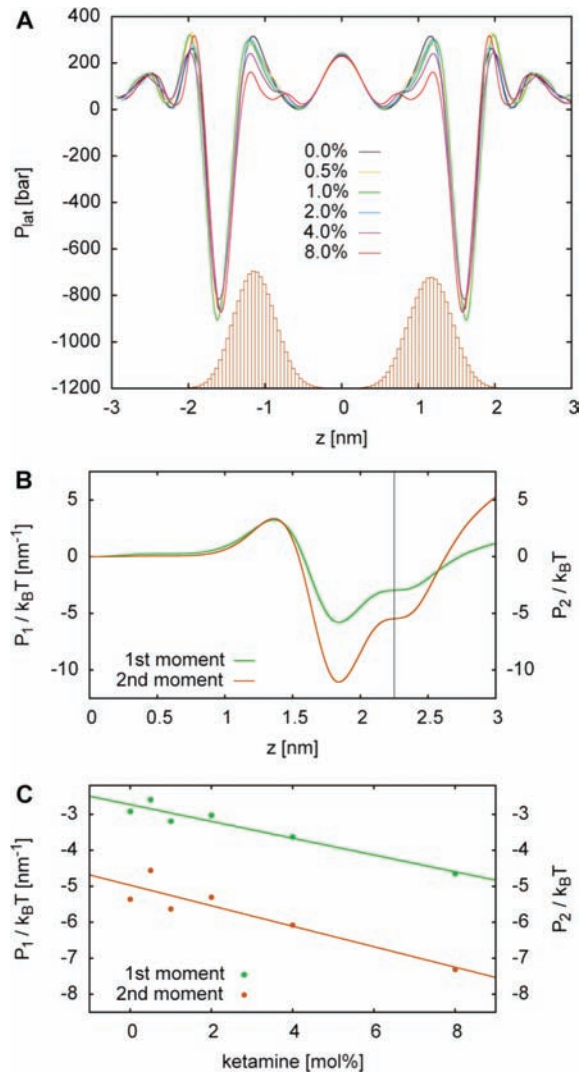

Figure 8. (A) Depth-dependent lateral pressure at different ketamine concentrations; the ketamine electron density is shown in brown. (B) First and second moment of the lateral pressure of the unanesthetized membrane as a function of the upper integration limit. The vertical line indicates the presently applied limit. (C) Concentration dependence of the first and second moment of the lateral pressure.

applied integration limit $d_B/2 = 2.3$ nm, as defined from the MD electron density profiles (see above), lies well within a regime where the variation of cumulative integral function is almost flat, making P_1 and P_2 more reliable. For pure POPC, we find $P_1 = -3.0k_BT$/nm and $P_2 = -5.5k_BT$. These values are considerably less negative than calculations for different acyl chains applying a statistical thermodynamic lattice model (16:0 chains: $P_1 = -18.4k_BT$/nm, $P_2 = -34.1k_BT$; 18:1 chains: $P_1 = -15.7k_BT$/nm, $P_2 = -27.9k_BT$).[17] The reason is that headgroup interactions could not be included in the previous estimates. Upon the addition of ketamine both P_1 and P_2 decreased further in a linear fashion with slopes of $-0.24k_BT$/nm/mol % and $-0.29k_BT$/mol %, respectively (Figure 8C).

Consequences for Membrane Proteins. We estimated the lateral pressure induced changes in the opening probability of membrane ion channel using two simple models (Figure 2). We build these ion channel models based on bacterial homologues of the nAChR channel with different structural properties. (i) In the asymmetric tilted helix channel model (Figure 2A) the lower radius r_1 is 2.0 nm in the closed and 2.7 nm in the open

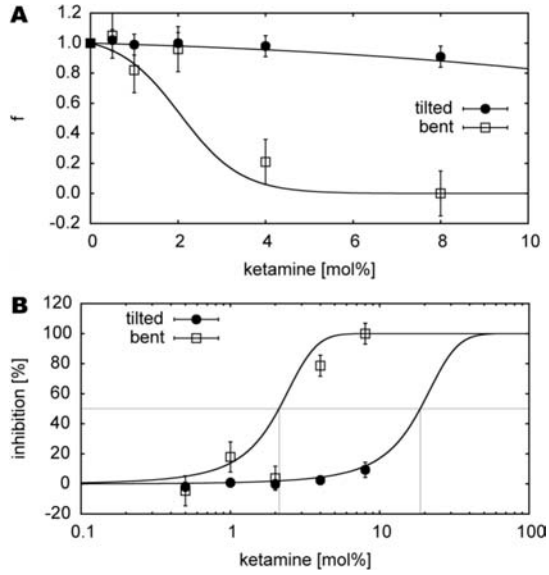

Figure 9. (A) Ketamine concentration dependence of the fraction of open channels. (B) Estimation of the percent inhibition. IC_{50} values for the two channel models are indicated by a gray line. Symbols represent data obtained using simulation results for P_1 and P_2. Solid lines were derived from the linear fits to these data (Figure 8C).

state, whereas the radius at the upper side was kept constant at $r_u = 2.7$ nm. (ii) In the symmetric bent helix model (Figure 2B), the upper and lower radius r_u was fixed at 2.5 nm, while the radius in the center of the channel (r_c) changes from 2.0 nm for the closed pore to 2.5 nm in the active state. The dependence of the fraction of open channels on drug concentration derived from eq 9 is shown in Figure 9A, assuming that in membranes 95% of the channels are in the open state ($K_0 = 5/95$) in the absence of ketamine. We found that the fraction of open channels decreased for both model proteins under the influence of ketamine induced lateral pressure changes. However, ketamine led to a more pronounced effect for the bent-helix model as the fraction (f) quickly approached zero at 8 mol % drug content, while f decreased moderately to 0.9 for the tilted-helix model at the same concentration.

In order to facilitate comparison with patch clamp experiments we derived the corresponding fraction of inhibited channels on a semilogarithmic plot (Figure 9B). For this purpose, we assumed that the linear dependencies of ΔP_1 and ΔP_2 (Figure 8C) persist to high ketamine concentrations. Our data indicate that activation of the bent-helix protein was quickly inhibited with a half-value of IC_{50} ~2 mol % ketamine, whereas ~18 mol % ketamine would be needed to close half of the tilted-helix protein.

Discussion

Development of compounds that allowed for anesthesia represented a major breakthrough for medicine, paving the ground for modern surgery. Nevertheless, our understanding of the mode of action of these remarkable molecules remains limited. This has led to a long history of scientific controversy. A nonspecific mechanism acting via the perturbation of the plasma membrane was the initially favored mechanism (see, e.g., refs 1 and 4). This was based on the observation of a strong correlation of the potency of anesthetics with their oil/water partition coefficient, which became known as the Meyer−Overton rule.[15,16] However, effects on membrane structural properties were found to be too small at clinically relevant concentrations of anesthetics, which was one of the major reasons to substitute the membrane mediated theory with a mechanism that requires specific interaction with ligand-gated ion channels.[64] Recently, membrane-mediated mechanisms have been revived,[8−10] and both schools of thought presently coexist within the scientific community.

The mechanism studied in the present work predicted a mechanical coupling of the conformational equilibrium of membrane proteins to depth-dependent changes of lateral pressures.[10] We put the prediction that is based on theoretical thermodynamic considerations to a test by combining experimental measurements with MD simulations. Further, we were using clinically relevant drug concentrations. In the first step, we verified the similarity of the anesthetic drug-induced effects on membrane structural parameters observed by the two approaches. Our combined efforts of SAXD and MD simulations did not show detectable changes of membrane thickness and area per lipid of POPC bilayers up to a concentration of 8 mol % (*R*)-(−)-ketamine. Similar results would have been taken previously as strong evidence against a membrane mediated mechanism of anesthesia. However, we were able to derive the corresponding lateral profiles $p_{LAT}(z)$ from the simulation data and observed drug induced changes of 100−200 bar at the membrane position that ketamine partitions to. This caused a net shift of lateral pressure toward the center of the POPC bilayer. Further, the changes in the first and second moments of the pressure profiles were found to decrease linearly within the studied ketamine concentration range.

These results allowed us to estimate the percentage of inhibited ion channels using two simple membrane protein models. We found significant effects even at low drug content and observed a dependency of the sensitivity to changes in the lateral pressure from the conformational changes involved. In the case of the bent-helix model, about 2 mol % of (*R*)-(−)-ketamine would have been sufficient to inhibit 50% of the channels models. Approximately 1 order of magnitude higher ketamine concentration would be required to achieve the same effect for the tilted-helix protein model (Figure 9B). These findings show that the anesthetic drug induced changes of the membrane lateral pressure profile might indeed contribute to changes of the conformational equilibrium of membrane-inserted ion channels.

Our protein models are designed to mimic the conformational change that accompany channel opening of the nAChR receptor as indicated by the bacterial homologues Glic[53] and Elic.[54] Two modes of channel opening seem likely. The channel could open by radially expanding at the intracellular site, as described by our model A. Alternatively, the conformational change of channel opening could involve bending of helices or changes in the tilt and relative helix orientation. Both transitions show overall shape changes as described in model B. Analysis of the structures of the bacterial homologues Elic and Glic suggests that the mode of channel opening is complex with contributions from model A and B. The two models might therefore represent extremes of the complex structural change of nAChR receptor gating.

It is instructive to compare the IC_{50} values of 2 and 18 mol % derived in this study to in vivo and in vitro data. These concentrations correspond to 34 and 365 μM solutions, respectively, within the hydrophobic membrane slab. If we assume

(64) Dayton, P. G.; Stiller, R. L.; Cook, D. R.; Perel, J. M. *Eur. J. Clin. Pharmacol.* **1983**, *24*, 825–831.

thermodynamic equilibrium, we can estimate the concentrations of unbound (*R*)-(−)-ketamine in the aqueous phase (bloodstream) to be 0.04 and 0.45 μmol/L, applying the octanol−water partition coefficient (log $P = 2.9$). About 50% ketamine is bound by protein in human plasma.[63] Therefore, at blood concentrations of ∼0.08 or ∼0.9 μM (*R*)-(−)-ketamine 50% of the bent or tilted helix model proteins, respectively, would be in the closed state.

In view of the simplicity and assumptions of our model system, the order-of-magnitude agreement with clinical data detailed below is encouraging. (*R*)-(−)-ketamine concentrations of 8 μM have been reported to be required for anesthesia in surgery.[65] Further, the blood concentration of ketamine racemic mixtures upon awaking was reported to range between 2.7 and 4.7 μM[66,67] and plasma concentrations between 0.17 and 0.63 μM were measured during analgesia experiments.[68−70] In vitro studies reported that ketamine reduced ion currents of NMDA and nAChR receptors in the same concentration range. IC_{50} values of 24.4−26 μM were reported for (*R*)-(−)-ketamine on inhibition the NMDA receptor,[71] while an IC_{50} of 0.24 μM was found for nAChR channel blockage using racemic ketamine.[72]

Conclusion

We have provided the first direct evidence that the insertion of anesthetic drugs into membranes does change the membrane lateral pressure profile already at clinically relevant concentrations without significantly affecting several other structural membrane parameters. We estimate that the effect is large enough that it could subsequently modulate the activity of membrane inserted ion channels by affecting their opening probability. Future studies need to address effects from membrane lipid composition[73] and increase the complexity of the protein models. The agreement of our order-of-magnitude estimates of IC_{50} values with concentrations found in clinical studies is encouraging.

Acknowledgment. We thank E. Lindahl for kindly providing us with the modified Gromacs version for evaluation of the lateral pressure profiles.

JA910843D

(65) Wachtel, R. E.; Wegrzynowicz, E. S. *Br. J. Pharmacol.* **1992**, *106*, 623–627.
(66) Little, B.; Chang, T.; Chucot, L.; Dill, W. A.; Enrile, L. L.; Glazko, A. J.; Jassani, M.; Kretchmer, H.; Sweet, A. Y. *Am. J. Obstet. Gynecol.* **1972**, *113*, 247–260.
(67) Idvall, J.; Ahlgren, I.; Aronsen, K. R.; Stenberg, P. *Br. J. Anaesth.* **1979**, *51*, 1167–1173.
(68) Clements, J. A.; Nimmo, W. S. *Br. J. Anaesth.* **1981**, *53*, 27–30.
(69) Grant, I. S.; Nimmo, W. S.; Clements, J. A. *Br. J. Anaesth.* **1981**, *53*, 805–810.
(70) Leung, A.; Wallace, M. S.; Ridgeway, B.; Yaksh, T. *Pain* **2001**, *91*, 177–187.
(71) Liu, H. T.; Hollmann, M. W.; Liu, W. H.; Hoenemann, C. W.; Durieux, M. E. *Anesth. Analg.* **2001**, *92*, 1173–1181.
(72) Flood, P.; Krasowski, M. D. *Anesthesiology* **2000**, *92*, 1418–1425.
(73) Cantor, R. S. *Biophys. J.* **1999**, *77*, 2643–2647.